International Journal of High-Rise Buildings
December 2021, Vol 10, No 4, 299-310
https://doi.org/10.21022/IJHRB.2021.10.4.299

International Journal of
High-Rise Buildings
www.ctbuh-korea.org/ijhrb/index.php

Upward Flame Spread for Fire Risk Classification of High-Rise Buildings

Martyn S. McLaggan[1,2], Vinny Gupta[1], Juan P. Hidalgo[1], and Jose L. Torero[3]

[1]*School of Civil Engineering, The University of Queensland, Australia*
[2]*Department of Civil & Structural Engineering, University of Sheffield, UK*
[3]*Department of Civil, Environmental & Geomatic Engineering, UCL, UK*

Abstract

External fire spread has the potential to breach vertical compartmentation and violate the fire safety strategy of a building. The traditional design solution to this has been the use of non-combustible materials and spandrel panels but recent audits show that combustible materials are widespread and included in highly complex systems. Furthermore, most jurisdictions no longer require detailing of spandrel panels under many different circumstances. These buildings require rapid investigation using rational scientific methods to be able to adequately classify the fire risk. In this work, we use an extensive experimental campaign of material-scale data to explore the critical parameters driving upward flame spread. Two criteria are outlined using two different approaches. The first evaluates the time to ignition and the time to burnout to assess the ability for a fire to spread, and can be easily determined using traditional means. The second evaluates the preheated flame length as the critical parameter driving flame spread. A wide range of cladding materials are ranked according to these criteria to show their potential propensity to flame spread. From this, designers can use conservative approaches to perform fire risk assessments for buildings with combustible materials or can be used to aid decision-making. Precise estimates of flame spread rates within complex façade systems are not achievable with the current level of knowledge and will require a substantial amount of work to make progress.

Keywords: Façade, Fire, Risk, Cladding, Upward flame spread

1. Introduction

External fire spread is a critical fire risk to assess and mitigate because it has the potential to breach vertical compartmentation. This is especially important for high-rise buildings where evacuation times are long, firefighting may be difficult or impossible and other layers of protection may also be ineffective, as described by Torero (2018). The traditional fire safety strategy mitigated this risk through the specification of strictly non-combustible materials, and adequately designed spandrels. Even with no combustible materials present, potential fire spread must be accounted for through thin cavities or openings forming from thermomechanical deflection e.g. at the floor-wall joint in curtain wall systems. Glazing and windows that can be opened also have to be considered.

The rise of the continuous external building envelope has led to the use of highly complex façade systems that many times include combustible components. These buildings may have the potential for external fire spread but the fire safety strategy intended to deliver life safety was not designed for this. As a result, investigation and remediation for tens of thousands of buildings across the world are required. A detailed background to the problem is given by McLaggan *et al.* (2021).

The testing practices, data and knowledge required to assess the risk of external fire spread are not yet at a level capable of evaluating highly complex façade systems as used in high-rise buildings. Flame spread itself is such an intricate phenomenon that even characterising turbulent upward flame spread on a simple solid surface is not completely solved. For downward flame spread, the potential for melting and dripping introduce phenomena which are exceedingly difficult to predict.

In this work, we explore some of the parameters influencing upward flame spread. We focus on upward spread because in most cases the spread rates are more rapid than downward spread, even if melting and dripping are considered. While dripping and melting are important mechanisms of fire spread that will have to be characterised, this mechanism is beyond the scope of this work. This is done only for simplicity and to take a step-by-step approach to the characterisation of this complex problem. The relative magnitudes of spread are shown in Figure 1 for four materials with a range of characteristics and which exhibit different burning behaviours as tested in a 600 mm intermediate-scale setup. This shows upward spread is around 4-18 times more rapid. The terminology, testing methodology, and materials are described in full later.

To explore the parameters of interest, the general flame

†Corresponding author: McLaggan, Martyn S.
Tel: +61-7-3365-3619
E-mail: m.s.mclaggan@sheffield.ac.uk

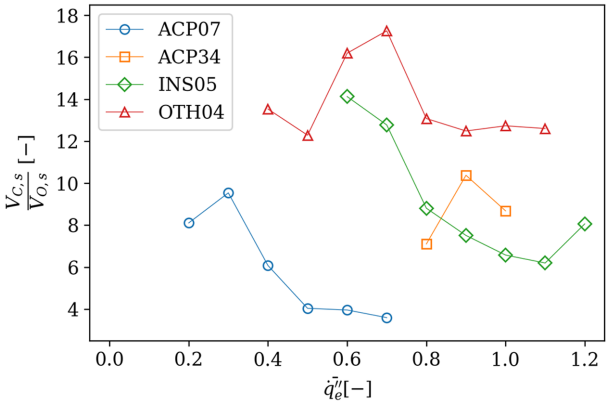

Figure 1: Ratio of concurrent (upward) flame velocities ($V_{C,s}$) to opposed (downward) flame velocities ($V_{O,s}$) as a function of the normalised heat exposure defined in Eq. (6).

spread equation for upward or wind-aided concurrent spread is given in Eq. (1) for a configuration shown in Figure 2:

$$V_s = \frac{4}{\pi}\frac{\delta_{ph}\dot{q}''^2_f}{k\rho c(T_{ig}-T_0)^2} \tag{1}$$

Where V_s is the flame spread velocity, δ_{ph} is the preheated length, $\dot{q}''_f$ is the heat flux from the flame to the fuel, $k\rho c$ is the lumped thermal inertia, T_{ig} is the ignition temperature, and T_0 is the initial temperature, taken as ambient (20°C). The constant $4/\pi$ represents a multiplication factor for the preheated length that emerges from the solution to the ignition delay time derived by Quintiere, Harkleroad and Hasemi (1986) from a semi-infinite solid transient heating analysis. This constant is not present in earlier formulations of upward flame spread e.g. Sibulkin and Kim (1977).

The flame heat flux is assumed to be constant over the preheated length. Values for the flame heat flux in concurrent spread typically vary from 25-35 kW m^{-2} as tabulated by Tsai *et al.* (2003), who went on to find that the best fit for models was around 15-20 kW m^{-2}. There is also some evidence for much larger values – up to 120 kW m^{-2} – as the burning rate increases and generally represents very large fires (Back *et al.*, 1994). Nevertheless, these values are generally only attained for a very small region over the pyrolysis length. The value selected here is 35 kW m^{-2}, which is more conservative than common analyses such as Tsai *et al.* (2003). This is higher than the critical heat flux for flaming ignition $\dot{q}''_{0,ig}$ required to ignite most solid fuels and is suitable to evaluate the short time small-scales near the onset of flame spread. If $\dot{q}''_f > \dot{q}''_{0,ig}$ then this is not a limiting factor to flame spread.

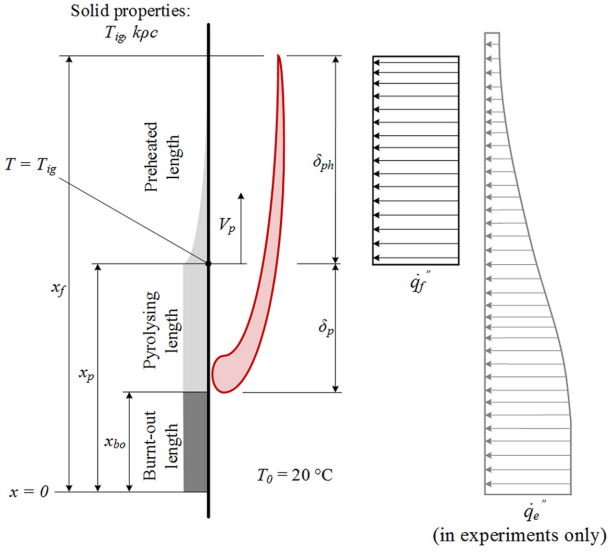

Figure 2. Upward flame spread.

The denominator in Eq. (1) denotes global material properties ($k\rho c$ and T_{ig}) and will vary the ease of ignition and hence the rate of flame spread.

The preheated length is defined in Eq. (2) as:

$$\delta_{ph} = x_f - x_p \tag{2}$$

Where x_f is the flame length and x_p is the pyrolysis length. If a stage is reached where $x_f \leq x_p$ then $\delta_{ph} = 0$ and the flame will not spread any further. This is the first of our limiting conditions for upward flame spread.

Saito, Quintiere and Williams (1986) use an identical form of Eq. (1 to define upward flame spread which can be checked by substituting Eq. (4) into Eq. (3):

$$V_p = \frac{dx_p}{dt} = \frac{x_f - x_p}{\tau_{ig}} \tag{3}$$

$$\tau_{ig} = \frac{\pi}{4}\frac{k\rho c(T_{ig}-T_0)^2}{\dot{q}''^2_e} \tag{4}$$

Where the time to ignition, τ_{ig}, is based only on the material properties and can be determined at a specific external heat flux, $\dot{q}''_e$. By inputting $\dot{q}''_e = \dot{q}''_f = 35$ kW m^{-2} an ignition time for upward flame spread can be derived.

The above considers that flame spread is always progressing and no burnout is considered. To properly establish limiting conditions of upward flame spread, the burnout front should be considered but this is not trivial to include and increases the complexity of solutions. In a similar manner to Eq. (3), a burnout front can be defined (T. G. Cleary and Quintiere, 1991; Mowrer and Williamson, 1991) in Eq. (5):

$$V_b = \frac{dx_{bo}}{dt} = \frac{x_p - x_{bo}}{\tau_{bo}} \tag{5}$$

Where x_{bo} is the burnout length and τ_{bo} is the burnout time. Flame spread is predicted to cease once the condition $V_p < V_b$ is met as the burnout front will eventually reach the

pyrolysis front and there will be no burning area remaining. By making $\frac{V_p}{V_b}<1$ and substituting equations (3) and (5), we discover that the ratio τ_{ig} / τ_{bo} will be a limiting condition and serves as a means to evaluate the propensity of upward flame spread.

From this, we conclude that we need to evaluate the following two conditions:

- Condition 1: $\frac{\tau_{ig}}{\tau_{bo}}>1$, in cases where the time to ignition is longer than the time to burnout, this is expected to lead to extinction. These parameters can be evaluated at bench-scale across a range of incident heat fluxes in a vertical orientation. If $\frac{\tau_{ig}}{\tau_{bo}}>1$ at $\dot{q}''_e = 35$ kW m^{-2} then the pyrolysing length, $x_p - x_{bo}$, will shrink and flames will not spread. It is important to note that the sample has to be a realistic or worst-case representation of the system that needs to be analysed. This will be discussed later. The notation used here is that τ_{bo} is measured from the onset of ignition (as opposed to the start of the test), so that at $t = \tau_{ig}$ then $\tau_{bo} = 0$.
- Condition 2: $\delta_{ph} = 0$. The evolution of x_f and x_p as a function of time will show whether the tendency is for $x_f \leq x_p$ or $x_f \geq x_p$. If the tendency is for $x_f \leq x_p$ then flame spread will cease. Evaluation of this requires an ad hoc test in the vertical orientation where both x_f and x_p can be recorded, and different ignition strengths are required to fully assess this parameter.

2. Material properties – ignition and burnout

Detailed flammability data is available from the Cladding Materials Library (McLaggan et al., 2021, 2019b). This contains a range of materials and the data includes chemical composition, thermal degradation, bomb calorimetry, ignitability, burning behaviour, and flame spread characteristics. The full framework and methodology are published (Hidalgo et al., 2019; McLaggan et al., 2019a).

The ignition and burning behaviour measurements taken were performed in the cone calorimeter across multiple heat fluxes ($\dot{q}''_e = 35$, 50 and 60 kW m^{-2}) in the horizontal orientation. The critical heat flux for flaming ignition, $\dot{q}''_{0,ig}$, was determined in further experiments by decreasing the heat flux iteratively until ignition was no longer achieved. A one-dimensional semi-infinite heating analysis for a thermally thick solid was applied (Torero, 2016) to approximate the thermal inertia, $k\rho c$, and ignition temperature, T_{ig}, both of which are apparent material properties. A summary of some of the key data is given in Table 1, where the time to ignition and burnout are obtained at a heat flux of 35 kW m^{-2}, equal to our assumed value of $\dot{q}''_f$ earlier. Although the data is all published, generic descriptors are given to help readers quickly refer to materials, where ACP A2 is Aluminium Composite Panel (ACP) with a highly inorganic core; ACP A2/thin film is where the only combustible is a thin layer of adhesive on aluminium skins; ACP FR is ACP with fire retardants; ACP PE is ACP with a polyethylene core; phenolic and/or cellulose are types of composites; PIR is polyisocyanurate foam; PHF is phenolic foam; EPS is expanded polystyrene; PUR is polyurethane foam, GFRP is glass fibre reinforced composite; WPC is wood polymer composite; and sarking is a thin polypropylene/ aluminium weatherproofing membrane.

To demonstrate the fit of the ignition model, the following normalised scaling parameters are introduced in Eqs. (6) and (7) based on the work by Torero (2000):

$$\overline{\dot{q}}'' = \frac{\dot{q}''}{\dot{q}''_{0,ig}} \tag{6}$$

$$\overline{t} = \frac{t}{t_c} \tag{7}$$

Where $\dot{q}''_{0,ig}$ is the critical heat flux for flaming ignition, $\dot{q}''_{0,ig} = h_T(T_{ig} - T_0)$, h_T is the total heat transfer coefficient at ignition, and t_c is a characteristic time, $t_c = \frac{k\rho c}{h_T^2}$. The total heat transfer coefficient was found iteratively as a function of the surface temperature – as described in the full methodology (McLaggan et al., 2019a) – with resulting values in the range of 33.9-56.7 W m^{-2} K^{-1}.

The fit is shown in Figure 3 for all materials from the Cladding Materials Library. The diagram is expressed as $1/\sqrt{(t)}$ to form a straight line fit, where the thermal inertia is essentially the gradient and the critical heat flux for flaming ignition is at $\overline{\dot{q}}''_e = 1$. The fit is shown to be reasonably good across all heat fluxes, and represents suitable determination of material properties.

To evaluate Condition 1, the ratio t_{ig}/t_{bo} is plotted as a function of the external heat flux in Figure 4. Where $t_{ig}/t_{bo} > 1$, this represents that the time to ignition is longer than the duration of burning, and that upward flame spread is likely to prove difficult. From the data available, there are only three materials meeting this condition: ACP01, INS03 and SRK01-S1. For INS03, this is a type of polyester wool which is difficult to assess because upon heating the surface recedes and the time to ignition is increased. This effect is well known for receding and shrinking materials (T. G. Cleary and Quintiere, 1991). Similarly, SRK01-S1 is a shrinking material and proves difficult to evaluate. From Figure 4, other materials close to reaching the condition $t_{ig}/t_{bo} > 1$ are OTH01 (phenolic composite) and ACP10 (ACP A2/thin film).

From this condition, we can rank all the materials as shown in Table 1. This is however not sufficient in itself and the overall propensity for upward flame spread should include Condition 2, or other parameters. Nonetheless, we assume that $t_{ig} / t_{bo} > 1$ is a critical condition then most materials evaluated here show the possibility for sustained upward flame spread.

Table 1. Material properties from the Cladding Materials Library. Times to ignition and burnout and peak heat release rate are at incident heat flux, $\dot{q}_e'' = 35$ kW m^{-2}. Materials are ranked according to the ratio t_{ig}/t_{bo}.

Material ID	Type	$k\rho c$	T_{ig}	$\dot{Q}''_{max}$	t_{ig}	t_{bo}	$\frac{t_{ig}}{t_{bo}}$
-	-	kW^2 m^{-4} K^{-2} s	°C	kW m^{-2}	s	s	-
ACP01	ACP A2	1.348	539	50	252	117	2.15
INS03	Polyester wool	0.733	530	317	163	117	1.39
SRK01-S1	Sarking	0.127	344	125	48	47	1.02
OTH01	Phenolic	1.613	502	91	630	902	0.70
ACP10	ACP A2/Thin film	0.466	376	215	37	63	0.59
ACP06-S1	ACP A2/Thin film	0.378	519	138	60	155	0.39
ACP02	ACP FR	1.643	378	117	144	407	0.35
INS04	EPS	0.531	434	228	62	208	0.30
ACP03	ACP PE	0.632	398	640	72	268	0.27
OTH23	GFRP	0.925	358	269	100	380	0.26
ACP09	ACP FR	1.856	407	135	183	910	0.20
ACP07	ACP PE	0.535	353	408	64	346	0.18
ACP22	ACP FR	1.878	371	115	159	901	0.18
ACP15	ACP FR	1.309	502	137	198	1372	0.14
ACP34	ACP FR	1.526	388	138	132	916	0.14
ACP05	ACP FR	1.227	393	160	114	896	0.13
ACP35	ACP FR	1.125	413	169	130	1035	0.13
ACP11	ACP FR	1.112	401	201	104	941	0.11
OTH04	Plywood	1.180	315	222	72	693	0.10
ACP04	Cellulose/phenolic	0.728	433	193	84	971	0.09
OTH24	WPC	0.663	423	198	98	1997	0.05
INS05	PIR	0.144	326	223	6	149	0.04
INS02	PHF	0.080	417	62	8	223	0.04
INS06	PUR	0.092	399	287	10	365	0.03
INS01	PIR	0.037	458	147	6	244	0.02
INS12	PUR	0.084	336	173	4	183	0.02

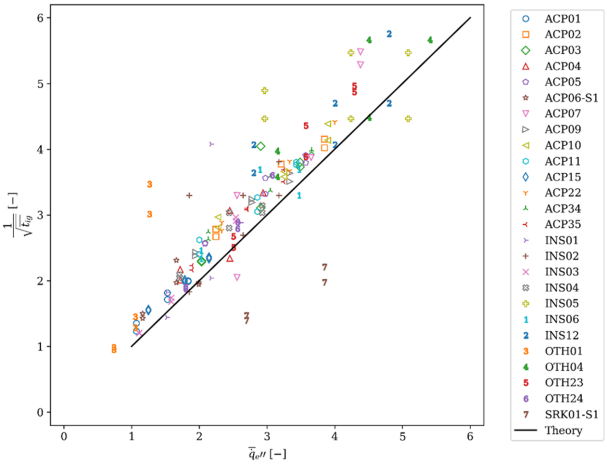

Figure 3 Normalised ignition diagram with experimental results and flaming ignition theory. Some results for SRK01-S1 at $\dot{q}_e''$ = 6 have been cropped.

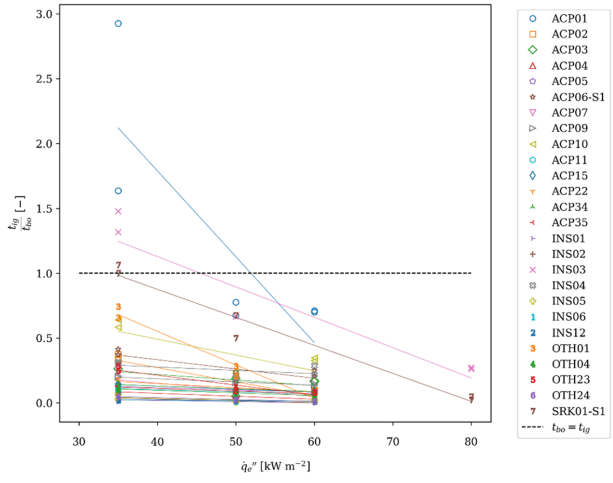

Figure 4. The ratio t_{ig}/t_{bo} for a range of external heat fluxes.

3. Preheated flame length

Flame spread measurements are available for the same materials. A modified version of ASTM E1321 (ASTM International, 2013; Quintiere, 1981) based on the original research methodology (Quintiere and Harkleroad, 1985) was performed on reduced-scale specimens (Long et al., 2000) in vertical orientation. Samples were 600 mm high and 100 mm wide, exposed to a radiant heat flux decreasing over the height of the sample (Figure 2). As before, full details of the methodology and framework are published (Hidalgo et al., 2019; McLaggan et al., 2019a).

For all materials, the encapsulation is removed. For the ACPs, this means removal of the aluminium skin, and for the PIR and other insulations it means removal of the aluminium foil facing or metal sheet. This provides a worst-case scenario and enables proper fire risk classification of materials. The inclusion of the full encapsulation, as a means of protection, increases the complexity of the problem by introducing mechanical modes of failure that require a full understanding of the thermo-mechanical behavior of the system. Thus, the present approach provides a conservative yet simplified approach that makes the problem tractable without full system experimentation. Therefore, the data from these tests does not represent a failure criterion for a system but provides valuable information required for a comprehensive risk assessment. Such risk assessment is outside the scope of work here.

Although the experimental setup may seem simple in principle, the nature of turbulent upward flame spread results in behaviour that is not trivial to evaluate. Given the complexity of analysis, we focus on only four distinct materials to explore the tendency of the preheated length. The materials are ACP07 (near pure polyethylene, a thermoplastic) with very high burning rate, INS05 (PIR insulation) with incredibly low thermal inertia, OTH04 (plywood) a well characterised charring material, and ACP34 (a charring ACP with Mg-based FR).

We illustrate the process of extracting the flame front, pyrolysis front and burnout front for one sample, INS05 (PIR), shown in Figure 5. Prior to starting the experiment, the specimen is marked at 25 mm intervals in alternating colours. This frame is extracted and used as the distance calibration. At the start of an experiment, the sample is preheated until the surface temperature reaches an approximate steady state. This was confirmed in initial tests using thermocouples close to the surface, and in later experiments the characteristic time from Eq. (7) was used as a simpler surrogate to approximate when the steady state was reached. The sample was then ignited using a propane torch at the bottom 50-100 mm of the sample, in the region above the critical heat flux for flaming ignition. In later testing, a superior ignition method was used where the propane torch was quickly dragged along all pyrolysed material so that the test focused only on flame spread below the critical heat flux for flaming ignition. As PIR is a charring material, the preheating time was kept short to ensure that ignition could still occur. In other cases, preheating had to be shortened before the material melted significantly. A script was used to extract frames every y seconds (in this case every 2 s for

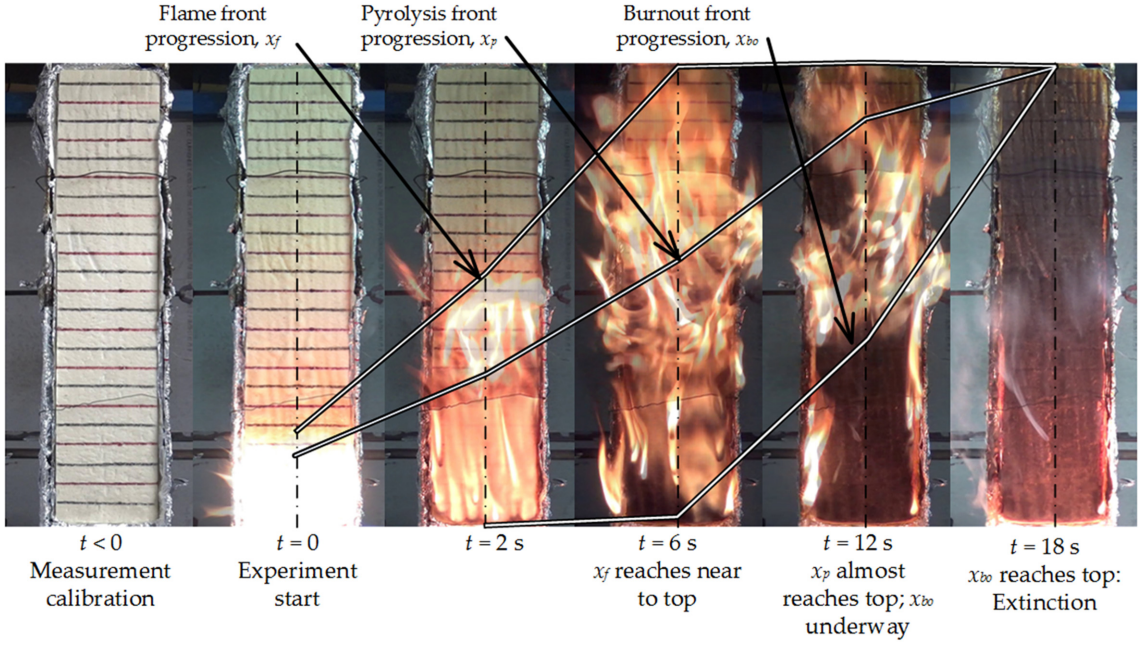

Figure 5. Illustration of front progressions in the experiment using snapshots of the sample taken at different timestamps. Three lines are overlain and annotated to roughly show the location of each front, and how it progresses between timestamps. This is for illustrative purposes only. The material is INS05, trial 02, and in the vertical orientation.

pyrolysis front, and 0.2 s for flame front). This pyrolysis front was taken as the location where flame attachment was clearly visible, or following a charring or melting front. While difficult to decipher from still images as in Figure 5, this process is markedly easier with the video as verification. It should still be appreciated that this is a difficult process. A side camera was also used to help identify the fronts. The flame length was taken as the highest point of the solid flame i.e. vortex shedding was not included, and the tip would lie in the intermittent region as defined by McCaffrey (1979). The contrast of the images was increased to help identify the flame. The detailed image processing approach at this point remains arbitrary and will require a thorough analysis. Given that this work aims at the presentation of the methodology and not the detailed results, the simple approach of a constant enhancement of the contrast was maintained. The burnout front has also been treated in a standardised yet approximate manner. The burn-out location was thus recorded as the location where the flame is extinct for the entire width of the sample, but flames sporadically emerging from cracks and edges, as well as molten droplets dripping off the sample have been ignored.

It should also be noted that a boundary layer flow established over a flat plate in natural convection transitions from laminar to turbulent (Bergman *et al.*, 2011). However, the presence of external heating by the radiant panel enhances pyrolysis rates of the fuel which results in a very complex interaction with the flow (Gupta *et al.*, 2021) thereby inducing strong turbulent flows (Tamanini, 1979). Therefore, the flames are expected to be mostly turbulent, particularly in the region where the flame spreads.

The results are shown in Figure 6. For each material, the flame progression until the top edge of the sample is recorded. Once x_f reaches this distance (i.e. when

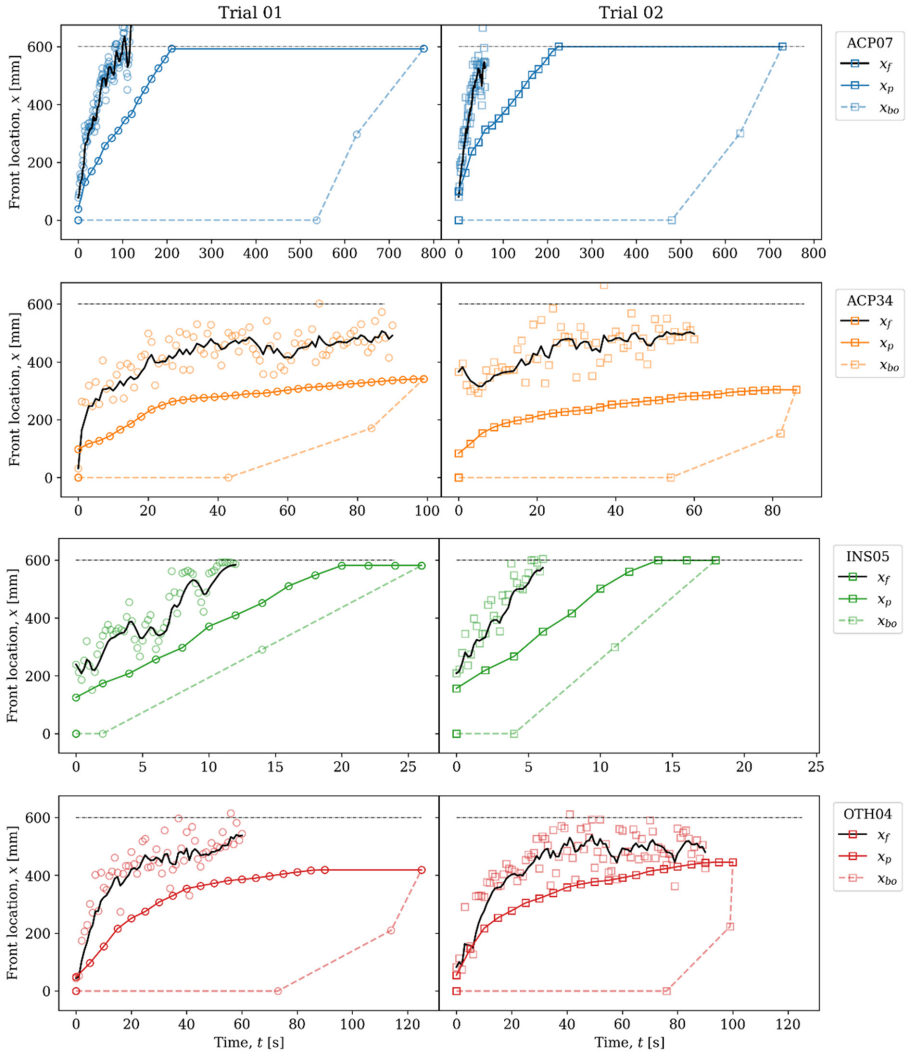

Figure 6. Flame fronts, pyrolysis fronts and burnout fronts for four materials (top to bottom), two trials each (left and right respectively). The flame reaches the top of the sample where $x = 600$ mm, marked with a dashed line. Black lines represent exponential weighted moving averages (10 points) to aid in locating the flame front.

$x = 600$ mm) then the conditions change. Until this point, x_f and x_p are free to grow as per Eq. (1). After this point, x_f is capped and δ_{ph} will forcibly be reduced. So, when the flame reaches the top surface, flame tracking is stopped.

3.1. ACP PE (ACP07)

The flame front consistently grows to the top of the surface within 80-100 s (Figure 6). The pyrolysis front also reaches the top surface, at approximately 200-250 s. After this point, the entire sample is burning freely and the flame height far exceeds the top surface, but this is not captured with the camera. Flaming nonetheless continues until extinction (marked by the progress of the burnout front), even though its progress after it reaches the top surface is not shown. Molten material spreads down the surface of the sample and burns, and as a result a burnout front is difficult to detect. The burning times recorded here are (550-800 s) are substantially longer than those recorded in the cone calorimeter (346 s, Table 1) due to this effect. In general, the behaviour is typical of a thermoplastic.

The behaviour of the preheated length, δ_{ph}, is that it consistently grows over time for the period measured (Figure 7). The energetic nature of the material with a high burning rate (Table 1) causes $x_f > x_p$ and suggests continued spread, especially given the long burning time.

3.2. ACP FR (ACP34)

The behaviour of the ACP FR is typical of a charring material (Figure 6). This is evident from the decay of x_p,

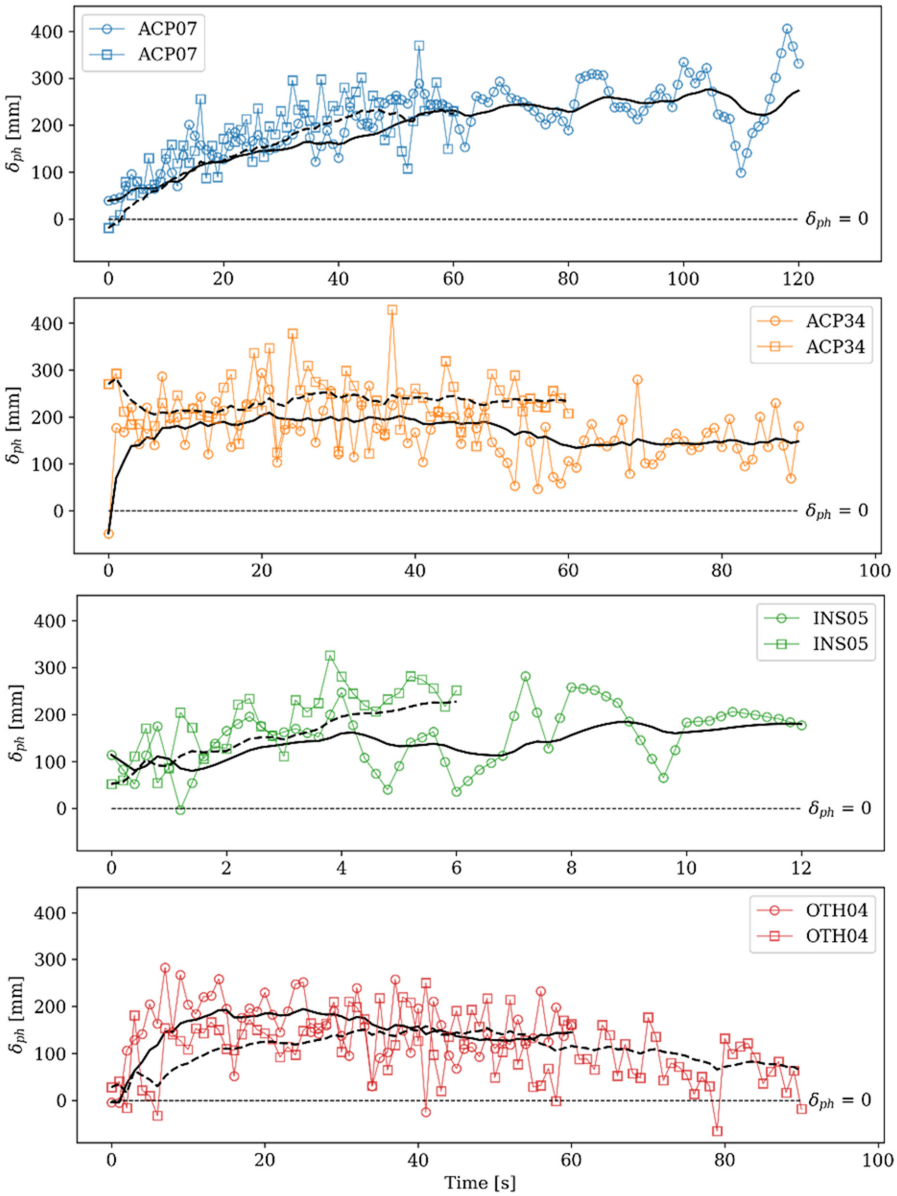

Figure 7. Preheated length as a function of time for four materials, two trials each. Black lines represent exponential weighted moving averages (10 points).

where the velocity (V_p) is initially high and eventually reaches zero. The charring nature of the material reduces the incident flux from the flame to the unburnt material, and reduces the velocity at which the flame spreads. The solid flame tip does not consistently reach the top surface of the apparatus, although in some cases the intermittent plume can be seen to exceed this limit. Flaming continues between 60 and 90 s in Trial 2 (until extinction) even though this is not presented here. This is due to the fact that the data was originally collected to measure the growth of the flame until its peak, as briefly explained earlier.

A burnout front initiates after around 40-55 s, although signs of flameout near the bottom of the sample are evident within the first 5-10 s. This may be because the heat flux from the flame to the bottom of the sample is very low, and cannot overcome the charring nature of the material. As the burnout front progresses, flaming becomes increasingly intermittent and extinction is rapidly achieved across the surface. This is evident from the gradient of the burnout front.

The preheated length, δ_{ph}, remains reasonably constant throughout the duration of the test (Figure 7). This indicates that the velocity is approximately steady (see Eq. (3), recalling that τ_{ig} is considered constant for a given material) and x_p may continue to grow. Given the charring nature of the material, it may also be possible that x_p stagnates and extinction is achieved within a reasonable distance.

This material undergoes melting due to the polyethylene component which, combined with the charring behaviour, can make characterisation challenging. This nature is true for many of the ACP FR-type materials as well as some other polymers e.g. PVC (polyvinyl chloride).

3.3. PIR (INS05)

The third material is a charring insulation with very low thermal inertia. Ignition and propagation are rapid, with the flame front reaching the top of the sample within 12 s (trial 1) or 6 s (trial 2). This behaviour is consistent with the flame spread equation as given in Eq. (1). The pyrolysis front also quickly reaches the top surface (within 14~20 s), and so the timescales for this material are clearly extremely short.

Progression of burnout front initiates shortly after ignition (4-5 s) and progresses steadily up the material. Extinction is reached after only 17-20 s, and much of the underlying material remains unburnt and protected by the char layer that has formed. Given the short burning duration and little material consumed, the energy release will be limited. Nonetheless, this material appears to easily support rapid fire spread.

Throughout the duration of the experiment, the preheated length grows (Figure 7) i.e. $x_f > x_p$. This supports the notation that this material can support flame spread and will be sustained.

3.4. Plywood (OTH04)

The flame front reaches a maximum through middle of the test and begins to recede (Figure 6). The flame front measurements in trial 1 stop at 60 s (approximately the maximum), but flaming continues until the end of the test at around 125 s in a similar fashion to trial 2 (where flame front tracking is stopped at 90 s). The pyrolysis front undergoes a period of initial growth, but as the char layer builds up in the preheated layer then the pyrolysis front velocity stagnates and x_p reaches a steady value. The approximation of the flameout front shows a front which accelerates rapidly until extinction is reached when $x_f \approx x_p$. This behaviour is more evident in Figure 7 where the preheated length growth is visible (0 to 20~40 s), before decaying for the rest of the test (20 s onwards in trial 1, and 40 s onwards in trial 2). The tendency here is typical of a charring material and eventually $x_p \geq x_f$, which leads to extinction and finite spread.

4. Scaling-up

The evaluation of Condition 1 and Condition 2 so far has suggested that a large number of materials in the Cladding Materials Library will be liable to spread flames. It is therefore important to understand how rapidly fire can spread beyond the scale of the experiment. To investigate the acceleratory nature of the materials, the linear flame approximation developed by Saito, Quintiere and Williams (1986) can be used. In Eq. (8):

$$x_f = K_f \dot{Q}''^{n} x_p \tag{8}$$

Where K_f and n are positive constants and $\dot{Q}''$ is the heat release rate per unit surface area of a material. The condition $x_f > x_p$ must be met for Eq. (8) to be valid. Different values for K_f and n have been reported in the literature. For example, using $K_f = 0.01$ m^2 kW^{-1} and $n = 1$ implies constantly accelerating spread, but will allow analytical solutions for the flame spread velocity. Using $K_f = 0.0067$ m^2 kW^{-1} and $n = 2/3$ introduces scaling to the heat release rate and may provide more realistic results, but ultimately always leads to extinction which proves problematic. This is discussed in more detail by Thomas (1994) and basic analysis of this dataset using Eq. (1) and Eq. (8) has already been performed (McLaggan et al., 2020).

Using this approximation, Saito, Quintiere and Williams (1986) eventually developed a Volterra type integral equation for upward flame spread in Eq. (9), with the full derivation being found in the literature.

$$V(t) = \frac{1}{\tau_{ig}}\left[k_f\left(\dot{Q}'_b + x_{p,0}\dot{Q}''(t) + \int_0^t \dot{Q}''(t-t_p)V(t_p)dt_p \right)^n - \left(x_{p,0} + \int_0^t V(t_p)dt_p \right) \right] \tag{9}$$

Where $\dot{Q}'_b$ is the heat release rate per unit length of a burner, $Q''(t)$ is the heat release rate per unit area from the material, $x_{p,0}$ is the initial pyrolysis length at $t = 0$, and t_p is a dummy variable of integration. The terms within the first set of rounded brackets () represent x_f, and the terms in second rounded brackets represent x_p.

Karlsson (1993), Thomas and Karlsson (1990), and others solved Eq. (9) analytically using Laplace transforms which required the introduction of a decay term, λ, to describe heat release data. This can be determined from cone calorimeter data by fitting $\dot{Q}(t)'' = \dot{Q}''_{max}\ e^{-\lambda t}$ for time past the peak heat release rate, and then taking the average value for λ. This allows the critical conditions to be identified using only bench-scale data, and can be illustrated using a plot first introduced by Baroudi and Kokkala (1992). The data from the Cladding Materials Library has been plotted in this manner in Figure 8. Numerical solutions are also possible and fairly straightforward by using the cone calorimeter data for $\dot{Q}(t)''$ directly and removing the need for the decay term. By doing this we would however not be able to explore the influence of each individual parameter as per the analytical solution and so this is not presented here.

The analytical predictions are shown in Figure 8. Additionally, the marker symbols are used to indicate the experimental results qualitatively – as described in the caption – so that the differences in the analytical predictions and experimental results can be compared. The term 'prediction' is used here loosely to mean an evaluation of the performance from the analytical solution, rather than a prediction of flame spread rates in real buildings. In cases where the flame spread reached the top of the sample in the experiment (filled symbols), it would be expected that these materials fall within Region I of the numerical predictions. Given the limited length of the sample, it is however possible that they could exhibit finite spread (Regions II) but there is insufficient length for this to be evident. Samples with finite spread in the experiment (hollow symbols) would be expected to fall within Regions II or III depending on the rate of spread and the final burnout location. The no spread materials (unfillable symbols) would be expected to fall within Region III. By comparing the symbol with the region that it lies within, we find that around all 10 materials that reached the top of the sample in the experiment were correctly predicted as accelerating by the numerical results. Of these, 6 out of 10 are within Region I which shows agreement between the experimental and numerical results. The remaining 4 out of 10 materials lie within Region II which may be a poor indicator of actual performance (underprediction of spread), and in particular 1 of these materials (ACP10) lies near the boundary with Region III suggesting a correct albeit poor prediction. For 10 out of 11 materials, finite growth is correctly predicted in some form, with OTH04 being the outlier which is incorrectly predicted as sustained acceleration. For the 5 samples with no spread in the experiment, 2 materials are correctly predicted as decelerating, 2 materials are borderline with finite spread, and 1 material (INS03) is incorrectly predicted as finite spread. In this manner, it is possible to identify that the numerical predictions give qualitative agreement in around 24 out of 26 materials. Of these, only 8 could

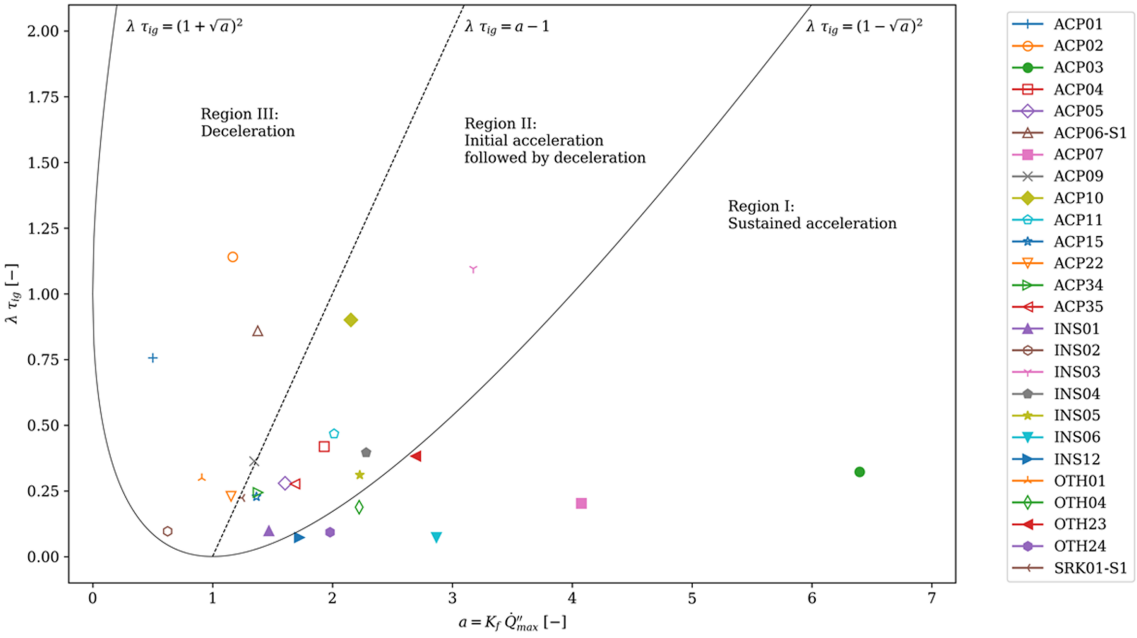

Figure 8. Analytical solutions of Eq. (9) applied to the experimental data. Filled symbols represent experimental data that reached the top edge, hollow symbols (e.g. empty circle) represent materials with finite spread, and unfillable symbols (e.g. cross) represent materials with no spread. Burnout is not considered.

be described as good agreement however. It should be remembered that this is intended as a tool to aid decision making and not a true numerical prediction, and the results are highly sensitive to the inputs. To explore the results in more detail, it is necessary to look at the individual materials and their performance.

Materials predicted to spread infinitely and rapidly match those that reached the top of the sample in the experiments presented in this paper. This was the case for materials with very large burning rates (ACP03 and ACP07, and OTH23 to a lesser extent), materials with extremely long burning durations (OTH24), and the insulations with both low thermal inertia and high burning rates (INS06 and INS12). Other insulations INS01, INS04 and INS05 are narrowly predicted incorrectly but lie so close to the region boundary that the prediction for most practical applications is still infinite spread. The prediction of rapid spread for plywood (OTH04) however does not match the experimental results, and does not match the literature. This is most likely because there is no consideration of burnout, and as a charring material this would likely lead to finite propagation. It may also highlight the sensitivity of these diagrams to the input parameters, as discussed by previous authors (Hasemi et al., 1994; Hasemi and Yasui, 1995). The cladding materials which contain only a thin layer of adhesive or polymer – ACP06-S1 and ACP10 – are both underpredicted, but as these are thermally thin then the analysis is not valid anyway so this would be expected. Materials with almost no spread in the experiments – ACP01, OTH01, ACP09 – all appear to be correctly predicted. The predictions for finite spread also seem reasonable. Groups of ACP FR show a spread of behavior with some potentially showing finite spread and others having only deceleration.

Table 2. Evaluation of properties to rank materials from the Cladding Materials Library, listed in order by Eq. (10).

Material ID	Type	$K_f \dot{Q}'' - \frac{t_{ig}}{t_{bo}} - 1$ Eq. (10)	V(t) Eq. (9)	$\frac{d\delta_{ph}}{dt}$ Exp.
INS02	PHF	–0.34	Deceleration	-
ACP22	ACP FR	0.33	Deceleration	-
INS01	PIR	0.49	Finite acceleration	-
ACP15	ACP FR	0.51	Finite acceleration	-
ACP02	ACP FR	0.52	Deceleration	-
ACP34	ACP FR	0.52	Finite acceleration	0
ACP09	ACP FR	0.55	Deceleration	-
OTH01	Phenolic	0.61	Deceleration	-
ACP05	ACP FR	0.73	Finite acceleration	-
INS12	PUR	0.75	Sustained acceleration	-
ACP06-S1	ACP A2/thin film	0.77	Deceleration	-
ACP35	ACP FR	0.81	Finite acceleration	-
ACP04	Cellulose/phenolic	1.02	Finite acceleration	-
OTH24	WPC	1.03	Sustained acceleration	-
ACP11	ACP FR	1.12	Finite acceleration	-
INS05	PIR	1.27	Finite acceleration	> 0
SRK01-S1	Sarking	1.27	Finite acceleration	-
OTH04	Plywood	1.33	Sustained acceleration	< 0
INS04	EPS	1.58	Finite acceleration	-
ACP01	ACP A2	1.66	Deceleration	-
ACP10	ACP A2/thin film	1.74	Finite acceleration	-
INS06	PUR	1.89	Sustained acceleration	-
OTH23	GFRP	1.96	Sustained acceleration	-
ACP07	ACP PE	3.26	Sustained acceleration	> 0
INS03	Polyester wool	3.57	Finite acceleration	-
ACP03	ACP PE	5.67	Sustained acceleration	-

As an aside, the results in Figure 8 tend to give better predictions if the decay factor, λ, is taken from cone calorimeter data at an incident heat flux of 50 kW m^{-2}, as opposed to 35 kW m^{-2} as per the rest of the data. Mowrer and Williamson (1991) encountered a similar effect in their numerical model built on Eqs. (3) and (5). They argued that the flame heat flux in the region $x_f - x_p$ is small and that small heat fluxes (e.g. < 35 kW m^{-2}) should be used for ignition criteria, while in the burning region $x_p - x_{bo}$, the flame heat flux is higher and should use data evaluated at higher heat fluxes (e.g. 50 kW m^{-2}). It is not particularly important here when used to qualitatively assess materials but may prove more significant when applying numerical models.

The analysis by Karlsson (1993) and others was focused on predicting flashover in the ISO 9705 (British Standards Institution, 1993) room corner test although it still fundamentally aims to predict whether or not acceleratory flame spread will occur for a given material. For upward flame spread, Hasemi *et al.* (1994) included limits for the ratio of the final pyrolysis height to the initial pyrolysis height, $x_{p,1}/x_{p,0}$, and plotted these on the Baroudi-Kokkala type plot. The limit for $x_{p,1}/x_{p,0} = \infty$ is already marked on Figure 8 as the intersection between Region II and I as this represents the transition to infinite spread. Within Region II, the ratio $x_{p,1}/x_{p,0}$ decreases the closer the material is to $a - 1 = \lambda\tau_{ig}$. According to the analysis by Hasemi *et al.* (1994), $a - 1 = \lambda\tau_{ig}$ on this diagram is very close to $x_{p,1}/x_{p,0} = 3$ in cases where the initial pilot flame is sustained and does not extinguish. This value suggests that the maximum rate of spread of that material would be triple the original pyrolysing length. Hasemi and Yasui (1995) described the analytical solutions in more detail, and discussed that direct measurement of $x_{p,1}/x_{p,0}$ in small-scale experiments may prove the best method to estimate performance. This is not altogether dissimilar to Condition 2 and the work presented in this paper.

The above analysis does not incorporate burnout and may yield inaccurate results. A number of authors have introduced a burnout term to Eq. (9) and solved the resulting equation (T. Cleary and Quintiere, 1991; Hasemi et al., 1994; Mowrer and Williamson, 1991). Despite the differing works, the limiting equation appears to be in the form given in Eq. (10):

$$K_f \dot{Q}'' - \frac{t_{ig}}{t_{bo}} - 1 \tag{10}$$

In cases where Eq. (10) > 1 then acceleratory spread is predicted to occur.

A summary of the prediction and experimental results are shown in Table 2. This serves as the basis for ranking materials to assist in fire risk classification. Material properties for the specific materials being considered must be determined from bench-scale experiments to be able to form any basis for a prediction. These properties can nonetheless be difficult to determine accurately, and prediction of behaviour such as Figure 8 is highly sensitive to the input. Furthermore, the determination of material properties tend to be apparatus dependent and care should be taken in their application. The direct evaluation of x_f and x_p in this work helps to bypass these challenges, and can be shown to describe the behaviour due to their fundamental influence on flame spread velocity, as represented in Eq. (1).

While many limitations of these different approaches have been presented in this section, it is clear that they all provide relevant and useful information that can be used by engineers in their assessment of the potential for vertical fire spread.

5. Conclusions

The ranking of cladding materials according to key upward flame spread parameters has been performed in this paper. This can be used to inform decision making of a competent fire safety engineer including the decision whether materials should undergo further testing to determine if their performance is suitable and will fit the strategy of a building being designed. As an example, the ACP PE materials (ACP03 and ACP07) clearly show unsatisfactory performance and there is little need to perform further testing. In contrast, both the ACP FR (ACP34) and plywood (OTH04) show better performance and therefore may represent suitable materials for a given building design. In this case, the data from these tests might be used in the analysis of a specific fire safety strategy or it would be worthwhile to perform further testing to complement this data. A similar conclusion can be reached for the PIR (INS05). The other 23 materials can be ranked in similar fashion, as well as future materials or materials not included here.

While the present paper does not aim to respond to design questions, it does aim to deliver a methodology that provides useful information for designers. The benefit of the approach here is that it relies on upward flame spread as its premise, rather than difficult to decipher pass/fail criteria or testing approaches which often do not evaluate suitably relevant parameters.

Acknowledgements

This work has been developed using resources from the *Material Library of Cladding Materials* (Grant No. 2018 001361) funded by the Queensland Government – Department of Housing and Public Works. Support from the Queensland Building & Construction Commission and Queensland Fire & Emergency Services as part of the Safer Buildings Taskforce is also gratefully acknowledged. All those who worked on the project as well as other members of UQ Fire are thanked. Dr Tuula Hakkarainen (VTT, Finland) is thanked for helping source literature.

References

ASTM International, 2013. E1321-13: Standard Test Method for Determining Material Ignition and Flame Spread Properties. https://doi.org/10.1520/E1321-13.1

Back, G., Beyler, C., Dinenno, P., Tatem, P., 1994. Wall Incident Heat Flux Distributions Resulting From An Adjacent Fire. Fire Saf. Sci. 4, 241-252. https://doi.org/10.3801/iafss.fss.4-241

Baroudi, D., Kokkala, M., 1992. VTT Publications 89: Analysis of Upward Flame Spread. Project 5 of the EUREFIC fire research programme. Espoo, Finland.

Bergman, T.L., Lavine, A.S., Incropera, F.P., DeWitt, D.P., 2011. Fundamentals of Heat and Mass Transfer, 7th ed. John Wiley & Sons, New York.

British Standards Institution, 1993. BS 476-33/ISO 9705 Fire tests on building materials and structures - Part 33: Full-scale room test for surface products. British Standards Institution.

Cleary, T., Quintiere, J., 1991. A Framework For Utilizing Fire Property Tests. Fire Saf. Sci. 3, 647-656. https://doi.org/10.3801/IAFSS.FSS.3-647

Cleary, T.G., Quintiere, J.G., 1991. Flammability Characterization of Foam Plastics. NISTIR 4664. Gaithersburg, MD. https://doi.org/10.6028/NIST.IR.4664

Gupta, V., Torero, J.L., Hidalgo, J.P., 2021. Burning dynamics and in-depth flame spread of wood cribs in large compartment fires. Combust. Flame 228, 42-56. https://doi.org/10.1016/j.combustflame.2021.01.031

Hasemi, Y., Yasui, N., 1995. A strategy to develop engineering upward flame-spread evaluation methodology based on the linearized flame height approximation. Fire Sci. Technol. https://doi.org/10.3210/fst.15.17

Hasemi, Y., Yoshida, M., Yasui, N., Parker, W., 1994. Upward Flame Spread Along A Vertical Solid For Transient Local Heat Release Rate. Fire Saf. Sci. 4, 385-396. https://doi.org/10.3801/IAFSS.FSS.4-385

Hidalgo, J.P., McLaggan, M.S., Osorio, A.F., Heitzmann, M., Maluk, C., Lange, D., Carrascal, J., Torero, J.L., 2019. Protocols for the Material Library of Cladding Materials -Part I: Framework, UQMLCM2019-01. St Lucia, Australia.

Karlsson, B., 1993. A mathematical model for calculating heat release rate in the room corner test. Fire Saf. J. 20, 93-113. https://doi.org/10.1016/0379-7112(93)90032-L

Long, R., Torero, J.L., Quintiere, J., Fernandez-Pello, A.C., 2000. Scale And Transport Considerations On Piloted Ignition Of PMMA. Fire Saf. Sci. 6, 567-578. https://doi.org/10.3801/IAFSS.FSS.6-567

McCaffrey, B.J., 1979. Purely Buoyant Diffusion Flames: Some Experimental Results (NBSIR 79-1910).

McLaggan, M.S., Hidalgo, J.P., Carrascal, J., Heitzmann, M.T., Osorio, A.F., Torero, J.L., 2020. Flammability trends for a comprehensive array of cladding materials. Fire Saf. J. 103133. https://doi.org/10.1016/j.firesaf.2020.103133

McLaggan, M.S., Hidalgo, J.P., Heitzmann, M., Osorio, A.F., Maluk, C., Lange, D., Carrascal, J., Torero, J.L., 2019a. Protocols for the Material Library of Cladding Materials - Part II: Sample preparation and testing methodologies, UQMLCM2019-02. St Lucia, Australia.

McLaggan, M.S., Hidalgo, J.P., Osorio, A.F., Heitzmann, M., Carrascal, J., Lange, D., Maluk, C., Torero, J.L., 2019b. The Material Library of Cladding Materials, Data Collection. https://doi.org/10.14264/uql.2019.441

McLaggan, M.S., Hidalgo, J.P., Osorio, A.F., Heitzmann, M.T., Carrascal, J., Lange, D., Maluk, C., Torero, J.L., 2021. Towards a better understanding of fire performance assessment of façade systems: Current situation and a proposed new assessment framework. Constr. Build. Mater. 300, 124301. https://doi.org/10.1016/j.conbuildmat.2021.124301

Mowrer, F., Williamson, R., 1991. Flame Spread Evaluation For Thin Interior Finish Materials. Fire Saf. Sci. 3, 689-698. https://doi.org/10.3801/IAFSS.FSS.3-689

Quintiere, J., 1981. A simplified theory for generalizing results from a radiant panel rate of flame spread apparatus. Fire Mater. 5, 52-60. https://doi.org/10.1002/fam.810050204

Quintiere, J.G., Harkleroad, M.T., 1985. New Concepts for Measuring Flame Spread Properties, in: Harmathy, T.Z. (Ed.), Fire Safety Science and Engineering, ASTM STP 882. Philadelphia, PA, pp. 239-267. https://doi.org/10.1520/STP35300S

Quintiere, J.G., Harkleroad, M.T., Hasemi, Y., 1986. Wall Flames and Implications for Upward Flame Spread. Combust. Sci. Technol. 48, 191-222. https://doi.org/10.1080/00102208608923893

Saito, K., Quintiere, J.G., Williams, F.A., 1986. Upward Turbulent Flame Spread. Fire Saf. Sci. 1, 75-86. https://doi.org/10.3801/IAFSS.FSS.1-75

Sibulkin, M., Kim, J., 1977. The dependence of flame propagation on surface heat transfer ii. upward burning. Combust. Sci. Technol. 17, 39-49. https://doi.org/10.1080/00102209708946811

Tamanini, F., 1979. A numerical model for the prediction of radiation-controlled turbulent wall fires. Symp. Combust. 17, 1075-1085. https://doi.org/10.1016/S0082-0784(79)80103-4

Thomas, P.H., 1994. On concurrent upward surface spread of flame. Fire Saf. J. 22, 89-99. https://doi.org/10.1016/0379-7112(94)90053-1

Thomas, P.H., Karlsson, B., 1990. On Upward Flame Spread On Thick Fuels, LUTVDG/TVBB--3058--SE. Lund, Sweden.

Torero, J.L., 2018. Grenfell Tower Inquiry: Professor Jose Torero expert report (Phase 1 - supplemental), JTOS0000001.

Torero, J.L., 2016. Flaming Ignition of Solid Fuels, in: SFPE Handbook of Fire Protection Engineering. Springer New York, New York, NY, pp. 633-661. https://doi.org/10.1007/978-1-4939-2565-0_21

Torero, J.L., 2000. Material Properties that Control Ignition and Spread of a Fire in Micro-Gravity Environments, ASME-NHTC-2000-12314, in: Proceedings of NHTC'00. Pittsburgh, Pennsylvania, p. 13.

Tsai, K.C., Turnbull, J., Will, G., Drysdale, D., 2003. Upward flame spread: Heat transfer to the unburned surface. Fire Saf. Sci. 117–128. https://doi.org/10.3801/IAFSS.FSS.7-117